

Dissipative Dynamics of Polymer Phononic Materials

*Original*

Dissipative Dynamics of Polymer Phononic Materials / Krushynska, Anastasiia O.; Gliozzi, Antonio S.; Fina, Alberto; Krushinsky, Dmitry; Battezzore, Daniele; Badilloávila, Miguel A.; Acuautla, Mónica; Stassi, Stefano; Noè, Camilla; Pugno, Nicola M.; Bosia, Federico. - In: ADVANCED FUNCTIONAL MATERIALS. - ISSN 1616-301X. - ELETTRONICO. - (2021), p. 2103424. [10.1002/adfm.202103424]

*Availability:*

This version is available at: 11583/2905352 since: 2021-06-09T13:01:19Z

*Publisher:*

WILEY-V C H VERLAG GMBH

*Published*

DOI:10.1002/adfm.202103424

*Terms of use:*

This article is made available under terms and conditions as specified in the corresponding bibliographic description in the repository

*Publisher copyright*

(Article begins on next page)



# Géotechnique

## **Chemo-mechanical behaviour of non-expansive clays accounting for salinity effects**

GEOT-2021-183 | Paper

Submitted by: Guido Musso, Giulia Scelsi, Gabriele Della Vecchia

Keywords: CLAY MINERALOGY, CONSTITUTIVE MODELLING, FABRIC/STRUCTURE OF SOILS, SUCTION, YIELD LOCUS

PDF auto-generated using **ReView**  
from





1

2           **Chemo-mechanical behaviour of non-expansive clays**  
3                           **accounting for salinity effects**

4

5           Guido Musso<sup>1</sup>, Giulia Scelsi<sup>2</sup> and Gabriele Della Vecchia<sup>3</sup>

6

7

8   1. Professor

9   Department of Structural, Geotechnical and Building Engineering

10   Politecnico di Torino

11   Corso Duca degli Abruzzi, 24

12   10129 Torino, Italy

13   [guido.musso@polito.it](mailto:guido.musso@polito.it)

14

15   2. Ph.D

16   Department of Civil and Environmental Engineering,

17   Politecnico di Milano

18   Piazza Leonardo da Vinci, 32

19   20133 Milano, Italy

20   [giulia.scelsi@polimi.it](mailto:giulia.scelsi@polimi.it)

21

22   3. Associate Professor

23   Department of Civil and Environmental Engineering,

24   Politecnico di Milano

25   Piazza Leonardo da Vinci, 32

26   20133 Milano, Italy

27   [gabriele.dellavecchia@polimi.it](mailto:gabriele.dellavecchia@polimi.it)

## 28 **Abstract**

29 Changes in the chemistry of the pore fluid are known to impact on the hydro-mechanical  
30 behaviour of clays. Experimental evidence collected in the last decades led to the formulation of  
31 constitutive chemo-mechanical models for expansive soils used in engineering practice for the  
32 containment of pollution, such as bentonite. Less attention has been paid to modelling the  
33 chemo-mechanical behaviour of non-expansive clays, less frequently used for geoenvironmental  
34 applications but equally exposed to chemical changes.

35 First key differences between the impact of salinity on the fabric of expansive and non-expansive  
36 clays are pointed out. At the macroscopic scale, an increase in salinity causes a small translation  
37 of the Normal Compression Line of non-expansive clays to higher void ratios, which in some cases  
38 is also accompanied by an increase in compressibility. The opposite occurs for expansive clays.  
39 These experimental evidences provide the basis for a chemo-mechanical model formulated in  
40 the frame of elasto-plasticity with generalised hardening, whose yield surface expands with pore  
41 fluid concentration. The model is validated against experimental results, both original and from  
42 the literature. Simulation results compare very well with those of tests performed on  
43 reconstituted, compacted and intact samples.

44

45

## 46 **1 - Introduction**

47 Pore fluid chemistry is well known to influence the hydraulic and mechanical behaviour of clays  
48 (see e.g. the comprehensive summary in Sridharan, 1991). This influence is due to the effects that  
49 the pore fluid composition has on superficial forces, such as van der Waals and electrostatic  
50 interactions, which act between close particles (see e.g. van Olphen, 1977,  
51 Santamarina et al., 2001). van der Waals interaction is always attractive and mainly depends on  
52 the dielectric constant of the pore fluid, while it is practically independent on the type and  
53 concentration of dissolved ions.

54 Electrostatic forces are caused by the electrical charge of the particle surface, and are mediated  
55 by the Diffuse Double Layer (DDL) of ions of opposite charge with respect to the one of the  
56 particle surface. As the solute concentration increases, the thickness of the DDL decreases and  
57 so do electrostatic forces. Particles of most clay minerals have a platy thin shape with large faces  
58 and thin edges. The electrical charge on the particles face is mainly caused by the isomorphous  
59 substitution in the crystal lattice of higher valence metals with lower valence metals (e.g. Mitchell  
60 and Soga, 2005): it is negative and not very influenced by pore water composition. The electrical  
61 charge on the particle edge is caused by the interruption of the crystal lattice, which exposes  
62 metals and hydroxyl groups to the surface: it is usually positive (van Olphen, 1977), and it can be  
63 influenced by the composition of the pore water because of the adsorption/desorption of  
64 protons and other ions (Santamarina et al., 2001). This is particularly relevant for kaolinite: as the  
65 pH grows the positive edge charge decreases and becomes negative at high pHs (e.g.  
66 Sposito 1984).

67 The interplay between van der Waals attractive forces and electrostatic forces (which are  
68 repulsive between particles faces, attractive between edges and faces) determines the type of  
69 association of the particles in suspensions and the fabric imparted through sedimentation.  
70 According to Santamarina et al. (2002), the ratio between the length and the thickness of the  
71 particles determines the relevance of the different forces. Particles of expansive clays, such as  
72 montmorillonite, are extremely elongated and thin. Edge charges have then very little relevance  
73 on their interaction and in suspensions they tend dispose according to a face to face association  
74 (i.e. they *aggregate*). This association dominates their fabric and as at high ionic concentrations  
75 more cations are available to shield the face negative charge the thickness of the double layer  
76 and the size of the pores in the aggregates reduces.

77 Particles of non-expansive clays, such as illite and kaolinite, have a smaller length to thickness  
78 ratio (i.e. they are relatively thicker) and attraction between particles edges and faces, or even  
79 between edges, can be relevant when they are in suspensions. The term flocculation is used to  
80 describe single particles, or groups of aggregated particles, associated according to a face to edge  
81 or edge to edge scheme. The association of kaolinite particles is ruled both by pH and ionic  
82 concentration (Palomino & Santamarina, 2005). Aggregation takes place above a threshold ionic  
83 concentration (NaCl molarity of the order of  $10^{-1}$  M): edge to face flocculation of aggregates  
84 occurs at both very low and very high pHs, while it has not been observed for pHs ranging  
85 between 5 and 7. Below the threshold ionic concentration aggregation occurs without  
86 flocculation when the pH is smaller than 3, while edge to face flocculation occurs at higher pHs.  
87 Not much attention has been paid to the role of pH for illite. As for the role of pore fluid salinity,  
88 the experience gathered for Norwegian illitic quick clays suggests that sedimentation in brackish

89 or marine water promotes edge to edge flocculation (i.e. a cardhouse type of fabric), which  
90 collapses after exposure to fresh water (see e.g. Rosenqvist, 1966). The same evidence has been  
91 reported for non-expansive smectites from Japan (Ariake clay, Ohtsubo et al.,1985).

92 The fabric of a given clay soil depends on the relative magnitude of superficial, body and  
93 mechanical forces when it is formed. While surface forces dominate on body and mechanical  
94 forces for suspensions and slurries, the opposite holds for compacted soils. The relevance of the  
95 soil formation stage, and in general of fabric, on the soil hydro-mechanical response has been  
96 clearly highlighted by Collins and Mc Gown (1974) according to which, although the fabric of soils  
97 *“cannot be expected to be determined simply on basis of the depositional history and*  
98 *environment, it has been found that there may be a dominant feature or set of feature present in*  
99 *any one soil. This predominant microfabric can induce certain types of engineering behaviors,*  
100 *such as sensitivity, collapse and expansion”*.

101 The impact of fabric on different aspects of the clay behaviour, and particularly on those related  
102 to the pore fluid chemistry imposed during preparation of reconstituted or compacted  
103 specimens, has been documented in many experimental works. The one-dimensional  
104 compression curves of samples reconsolidated from slurry have been found to depend on the  
105 pore fluid of preparation for kaolinite and bentonite saturated with fluids with different dielectric  
106 constant (Sridharan & Rao, 1973) and smectitic soils saturated with brines (Barbour & Yang, 1993,  
107 Di Maio, 1996). Barbour & Yang (1993) further remark that adding brine to montmorillonite  
108 material prior to static compaction in unsaturated conditions causes the moisture-density  
109 relationship to be altered due to physicochemical effects, which leads to compression curves  
110 which depend both on the preparation procedure and on the pore fluid chemistry.

111 Modifications of pore fluid chemistry are also possible due to pore fluid replacement or of  
112 diffusion of the solutes, and pore water chemistry is expected to change with time in many earth  
113 structures devoted to pollution containment. For example, in compacted clay barriers for nuclear  
114 waste storage, chemical changes can occur due to the inflow of water from the host rock and  
115 because of the evaporation triggered by temperature increase induced by radioactive reactions.  
116 In both cases, a variation of the concentration of the species dissolved in water is anticipated. In  
117 clay barriers for municipal waste disposal, the pore fluid chemical composition changes with the  
118 transport of domestic leachate, while cutoff walls encapsulating polluted sites can be  
119 progressively permeated by the contaminants spilled underground. Pore fluid chemistry also  
120 varies in natural environments, e.g. in clay formations that were deposited in marine  
121 environments that emerged in relatively recent geological times. After emersion, salt diffusion  
122 towards the boundaries of the formation or entrance of fresh water (i.e. leaching) are  
123 anticipated.

124 As changes in the pore fluid chemistry modify the interaction between particles, deformations  
125 even at constant total stress and impact on the hydro-mechanical properties are expected.  
126 Volume change caused by pore fluid replacement under a constant vertical stress and their  
127 effects on the following compression behaviour were studied among others by Sridharan & Rao  
128 (1973), Torrance (1974), Di Maio (1996), Musso et al., (2003, 2013). Torrance (1974) leached with  
129 distilled water undisturbed samples of Norwegian quick clays, originally filled with marine water:  
130 this process induced shrinkage in normally consolidated samples and swelling of highly over-  
131 consolidated samples.

132 To account for these effects, elastic-plastic chemo-hydro-mechanical models (e.g. Hueckel, 1997;  
133 Loret et al., 2002; Gajo & Loret, 2003; Liu et al., 2005; Guimaraes et al., 2013, Witteveen et al.,  
134 2013, Della Vecchia & Musso, 2016, Yan, 2018, Della Vecchia et al, 2019) were formulated in the  
135 past decades. Limited efforts have been devoted to modeling the behaviour of non-expansive  
136 clays, since excluding Witteveen et al.(2013) all of these works make specific reference to very  
137 expansive clays (bentonites, mostly relying on the experimental data from the seminal paper of  
138 Di Maio, 1996).

139 This work aims at formulating a simple phenomenological elasto-plastic model for the chemo-  
140 mechanical behaviour of non-expansive illitic and smectitic clays. First, the different effects of  
141 salinity on the behaviour of expansive and non-expansive clays are explored. The paper focuses  
142 then on non-expansive clays, exploring the relationship between pore fluid salinity, clay fabric  
143 and void space. The experimental behaviour of oedometer reconstituted samples of a smectitic  
144 non-expansive clay under the effects of mechanical loads imparted at different constant pore  
145 fluid compositions and of salinity changes imparted at constant vertical stress is discussed. The  
146 experimental results are exploited to formulate a constitutive model in the framework of elasto-  
147 plasticity with generalized hardening. The model was then used to simulate the results of  
148 experimental tests, both original and from the literature, performed on samples of different soils  
149 and with different initial fabrics (reconstituted from slurry, undisturbed and statically compacted  
150 samples). In all these cases, a very good agreement between model predictions and experimental  
151 data was found.

152

## 153 **2. Influence of pore fluid salinity on the liquid** 154 **limit of active and inactive clays**

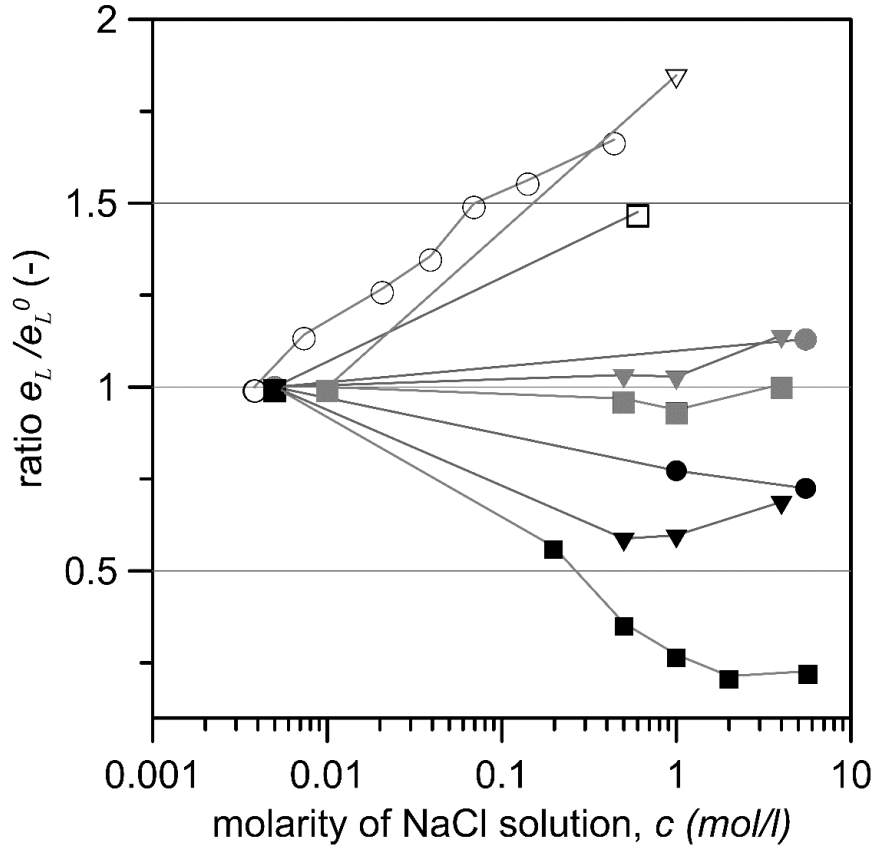
155

156 As recalled by Jang and Santamarina (2016), liquid limit determinations account for the mass of  
157 water which is both adsorbed onto the particle surfaces and held within the fabric. Comparing  
158 the liquid limits obtained using different saline solutions reveals then the impact of the pore fluid  
159 composition on the fabric of a given clay in slurry state. However, expressing the results of the  
160 liquid limit tests in terms of the ratio between the mass lost through heating in the oven to the  
161 non-evaporated mass is here inappropriate, since dissolved salts don't evaporate and they would  
162 be improperly considered as solid fraction. Furthermore, as the density of a solution depends on  
163 the solute concentration and the fabric is related to the type and volume of voids in the soil, the  
164 comparison between liquid limits at different salinities is more significant if expressed in terms  
165 of void ratio  $e_L$  instead of gravimetric water content  $w_L$ .

166 The effects of water salinity on the liquid limit was analysed for the soils listed in Table 1, where  
167 mineralogical compositions are also provided. The corrections required to the measurements of  
168 the mass lost in the oven were carried out accordingly to the procedure described in Noorany,  
169 1983. The data set includes pure clays (kaolinite, illite and bentonite), as well as natural soils from  
170 Italy, Norway and Japan. Both data from the literature and original determinations are  
171 considered. The original determinations include a pure illite from Hungary (provided by BAAN  
172 industrial materials, Formigine, Italy), a commercial sodium bentonite which was mixed with the  
173 illite (provided by Laviosa Chimica Mineraria, Livorno, Italy), and Spigno Monferrato clay, a  
174 natural clay proceeding from the Langhe region of Italy which has been the seat of diffuse slope

175 instabilities promoted by the dilution of the interstitial pore water (Musso et al., 2008; Musso et  
176 al., 2017). Spigno Monferrato is a mixture of nontronite (a non-expansive ferrous smectite), illite  
177 and chlorite.

178 Table 1 also reports the void ratio at liquid limit obtained mixing the powder of these clays with  
179 distilled water,  $e_L^0$ , which ranges from 0.80 (Asrum clay) to 10.80 (Ponza Bentonite). The  
180 normalised ratio  $e_L/e_L^0$  is then used in Figure 1 to show in a single graph the effects of salinity on  
181 the liquid limits of the different soils. Three different trends can be observed:  $e_L$  decreases with  
182 salinity in the case of pure expansive minerals (Ponza Bentonite) and of clays containing  
183 expansive minerals (75 illite 25 bentonite, Marino clay); it remains about constant or increases  
184 very mildly with salinity for Spigno Monferrato clay, illite and kaolinite; it increases sharply in the  
185 case of quick clays from Norway (Asrum and Drammen clay) and Japan (Ariake clay).



Expansive clays	Non expansive clays	Quick clays
■ Ponza bentonite	■ Spigno Monferrato	□ Asrum clay
▼ 75 Illite 25 Bentonite	▼ Illite	▽ Ariake clay
● Marino clay	● Kaolin	○ Drammen clay

186

187

188 Figure 1 – Dependency of the void ratio at liquid limit  $e_L$  on NaCl molarity of the pore fluid for  
 189 different clays  
 190

191

192

193

194 Table 1 – Mineralogy and index properties with distilled water as saturating fluid for different clay

195 soils

Soil	Reference	Main minerals	Liquid limit $w_L$ (%)	Void ratio at liquid limit with distilled water $e_L^0$ (-)
Ponza Bentonite	Di Maio (1996)	montmorillonite 80% kaolinite 20%	390	10.80
75 Illite – 25 Bentonite	This study	illite 75 % bentonite 25 %	161	4.43
Ariake clay	Ohtsubo et al. (1985)	beidellite type, non- expansive smectite 46% illite	89	2.54
Illite	This study	illite > 95 %	83	2.26
Kaolin	Di Maio et al (2004)	kaolinite 75-80% illite 8-10%	50	1.37
Marino clay	Di Maio et al. (2004)	kaolinite 30% illite 10 % mixed illite – expansive smectite 10%	50	1.52
Spigno Monferrato	This study	nontronite, non expansive smectite illite,	41	1.13

		chlorite		
Drammen clay	Torrance (1974)	Illite Chlorite	32	0.88
Asrum clay	Bjerrum and Rosenqvist (1956)	Illitic clay	29	0.79

196

197 The results for the expansive soils agree with the observations of Sridharan et al. (1986),  
 198 according to whom their liquid limit is mostly ruled by effect of the reduction with salinity of the  
 199 thickness of the double layer on the particles face. This appears not to be the case with the other  
 200 materials. The increase of  $e_L$  with salinity for the quick clays is consistent with the flocculated  
 201 fabric exhibited by these soils in saline water, which is lost upon exposure to fresh water  
 202 (Rosenqvist, 1966, Torrance & Ohtsubo, 1995). The flocculated fabric implies larger pores than  
 203 the aggregated fabric, explaining the increase of  $e_L$  with salinity. A similar phenomenon is  
 204 expected for the pure illite. While the liquid limit of kaolinite is controlled mostly by the pH while  
 205 it is not much affected by salinity alone (Sridharan et al., 1988), the kaolin considered in Figure 1,  
 206 proceeding from the work of Di Maio et al. (2004) contains a 10 % fraction of illite, which might  
 207 justify the increase of  $e_L$  with salinity, while the different behaviour of different minerals might  
 208 explain the trend of  $e_L$  for Spigno Monferrato clay, where  $e_L$  decreases slightly at lower salinities  
 209 and increases at higher salinities.

210

211

### 212 **3. Compression behaviour of non expansive** 213 **clays along chemo-mechanical paths**

214

#### 215 3.1 Elastic and elasto-plastic compliance along constant salinity paths

216

217 As salinity can impact on the fabric and liquid limit of clays, it is expected to affect also their  
218 behaviour along compression. The dependency of oedometer compressibility on the salinity  
219 (NaCl concentration) of the pore water for the soils listed in Table 1 and a few other materials  
220 from the literature is shown in Figure 2. All the samples considered were loaded while saturated  
221 with the water of preparation (i.e. no replacement of the pore fluid have been performed).  
222 Compressibility is here expressed in terms of elastoplastic and elastic logarithmic compliance,  $\lambda$   
223 and  $\kappa$  respectively:

224

$$225 \quad \lambda = - \frac{\Delta e}{\Delta \ln \sigma'} \quad (1)$$

$$226 \quad \kappa = - \frac{\Delta e}{\Delta \ln \sigma'} \quad (2)$$

227

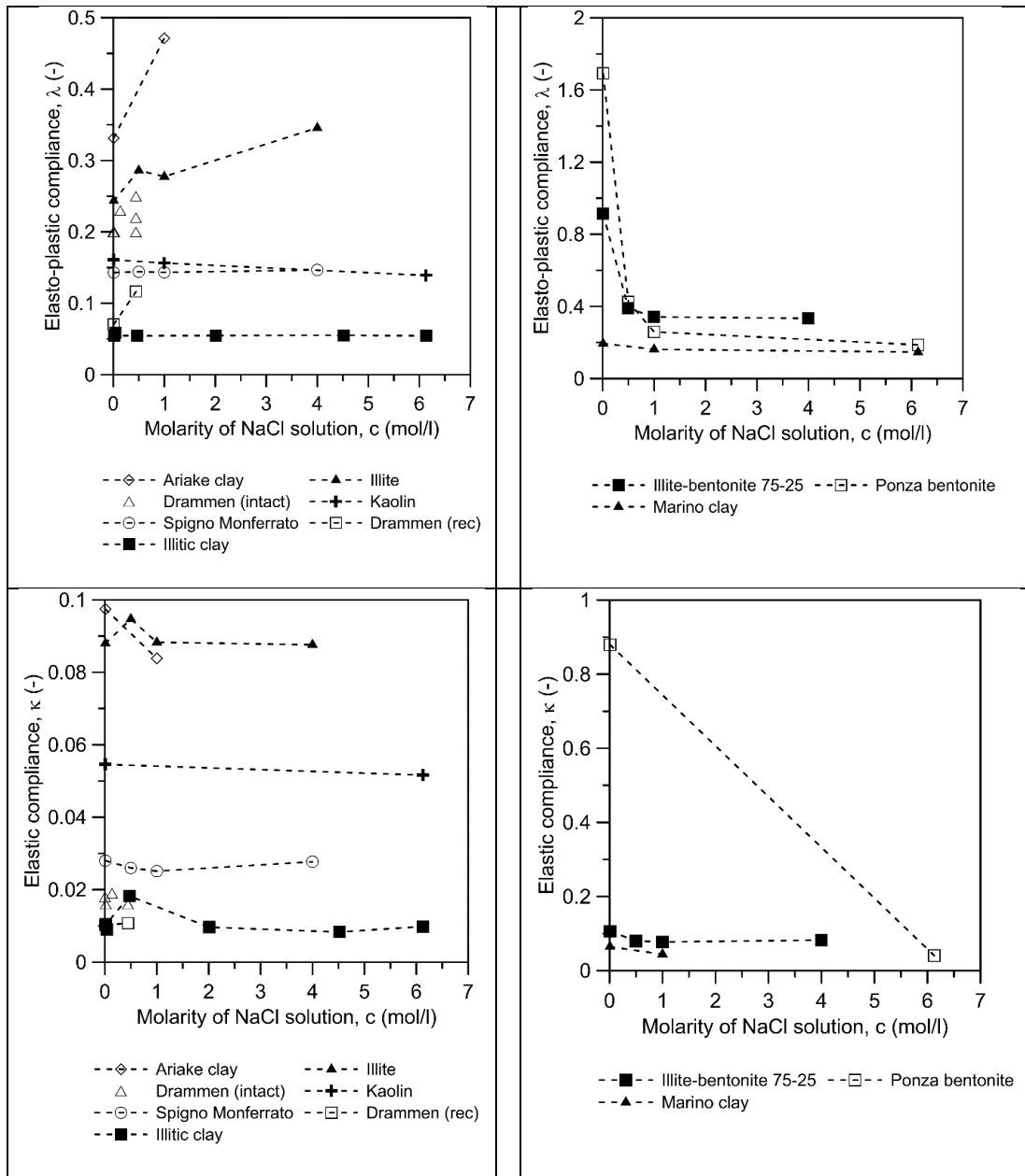
228  $\lambda$  was evaluated along the virgin loading branch in the stress range between 150 kPa and 300  
229 kPa, while  $\kappa$  was determined along the unloading branch. The relationship between  $\lambda$  and salinity  
230 is similar to the one between  $e_L$  and salinity:  $\lambda$  decreases dramatically with concentration for soils  
231 containing expansive minerals, it has a moderate increment with concentration for the illite and  
232 for the quick clays, and it remains about constant for kaolin and Spigno Monferrato clay. The  
233 influence of salinity on  $\kappa$  is generally very small. While most data refer to reconstituted  
234 conditions, Figure 2 also reports data of an intact sample of Drammen clay (Torrance, 1974) and

235 of a compacted low-activity illitic clay (Witteveen et al., 2013). The compliance of the intact  
236 Drammen clay is higher than the one of the reconstituted Drammen clay, but the role of pore  
237 fluid chemistry is similar, as  $\lambda$  moderately increases with the concentration in both cases. No  
238 measurable effects of the pore fluid concentration on compliance were found for the illitic clay  
239 in Witteveen et al. (2013). ù

240

241

242



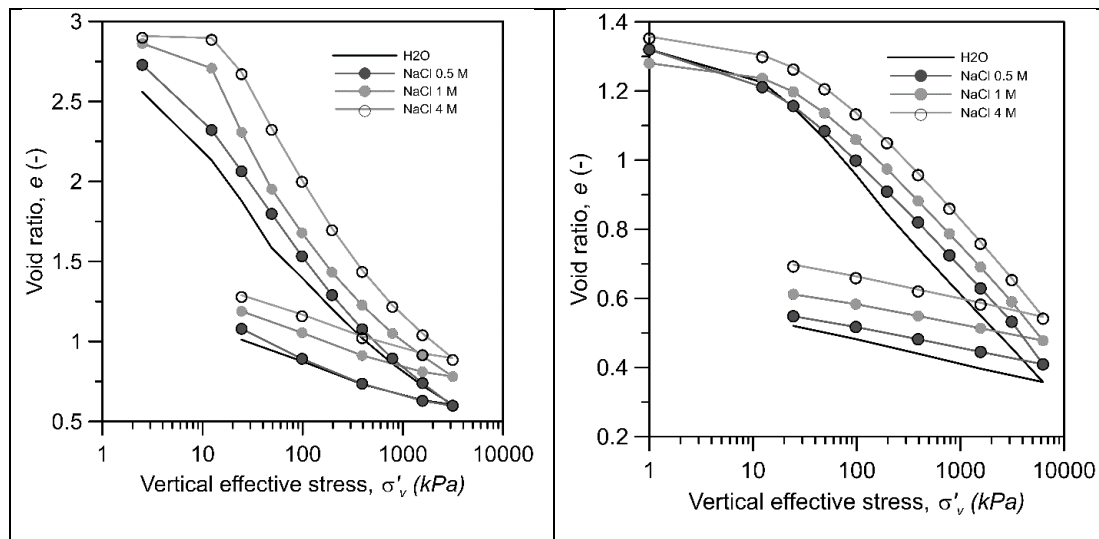
243

244 Figure 2 – Dependency of soil compressibility on NaCl molarity for different clays. (a) elasto-  
 245 plastic compliance of non-expansive clays, (b) elasto-plastic compliance of expansive clays, (c)  
 246 elastic compliance of non-expansive clays, (d) elastic compliance of expansive clays

247 3.2 Compression curves of non-active clays and relationship with fabric

248

249 The salinity of the pore water of preparation might affect the compression behaviour also by  
 250 impacting on the position of the Normal Compression Line (NCL), i.e. on the void ratio associated  
 251 to first loading under a given effective stress. Restricting the analysis to the soils tested in the  
 252 present work, Figure 3 provides the experimental results for the illite and Spigno Monferrato  
 253 samples. All the specimens were reconstituted and they were prepared by mixing the dry soil  
 254 powder with the mass fluid required to impose an initial void ratio  $e \cong 1.2 e_L$ . Distilled water and  
 255 NaCl solutions with different molarities (0.5 M, 1 M, 4M) were used. For both soils, salinity has a  
 256 small effect on  $\lambda$ , but its increase translates the NCL to higher void ratios. The opposite effect  
 257 occurs for expansive soils, whose NCL moves to lower void ratios as salinity increases (see e.g.  
 258 Di Maio, 1996).



259

260 Figure 3 – Oedometer compression curves of illite (left) and Spigno Monferrato clay (right)

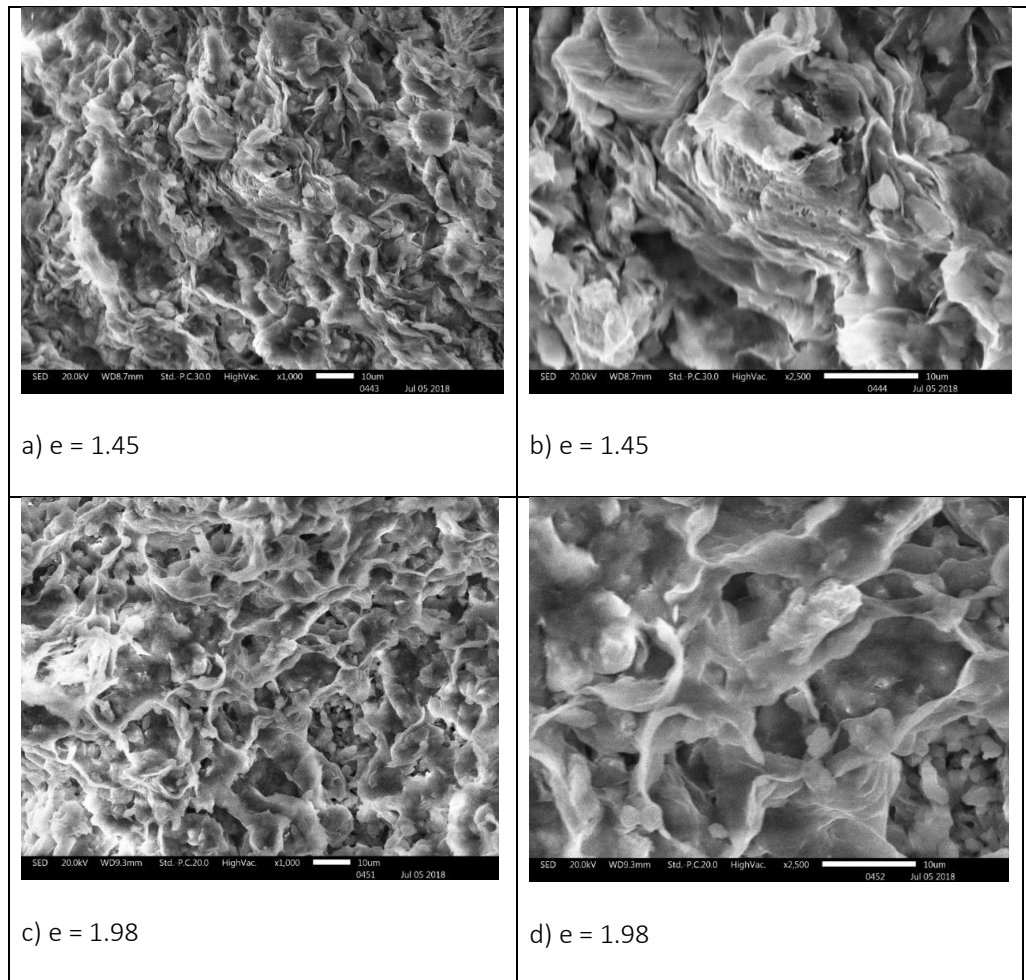
261

satuated with NaCl solutions of different molarity

262 The effects of salinity on the compression behaviour descend from the effects of salinity on  
263 fabric. Different microstructural analyses were conducted on specimens normally consolidated  
264 at a vertical stress  $\sigma'_v = 98$  kPa. All specimens were freeze dried before microscopic analysis, to  
265 avoid modifications of the pore network due to water evaporation in natural conditions.

266 Scanning Electron Microscope (SEM) images of the illite specimens prepared with distilled water  
267 and with the 4 M NaCl solution are presented in Figure 4. The differences between the two fabrics  
268 is very clear. The distilled water specimen (Fig. 4a and 4b) has a void ratio  $e = 1.45$  and its particles  
269 are mostly aggregated parallel one to the other in a face to face arrangement, with elongated  
270 pores whose main apertures have size of the order of about  $1 \mu\text{m}$ . The 4 M NaCl specimen (Fig.  
271 4c and 4d) has a larger void ratio  $e = 1.98$ . A cardhouse fabric emerges, with particles disposed in  
272 an edge to edge arrangement, forming larger pores with diameters of the order of  $5 - 10 \mu\text{m}$ .  
273 Notwithstanding the load that was applied, the flocculated fabric imparted to the specimen  
274 mixing the soil with highly saline water is still evident, which explains the higher void ratio of this  
275 specimen with respect to those prepared at lower salinities.

276



277

278 Fig. 4 SEM images of reconstituted illite specimens prepared at  $e = 1.2 e_L$  and loaded to 98 kPa.

279 Pore fluid is: (i) distilled water for images a) and b); (ii) 4 M NaCl solution for images c) and d).

280

Bar length is 10  $\mu\text{m}$  in all pictures

281

282 The effects of salinity on the fabric of Spigno Monferrato clay were investigated by means of

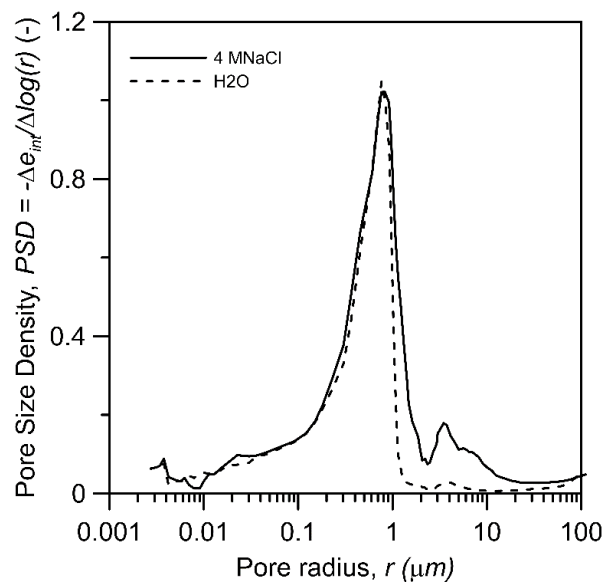
283 Mercury Intrusion Porosimetry (MIP) tests, performed on the specimens prepared with distilled

284 water and with the 4 M NaCl solution. The Pore Size Density function (PSD) curves of these

285 specimens are presented in Figure 5: they show a peak in correspondence of a pore radius slightly

286 smaller than 1  $\mu\text{m}$  and they almost overlap at smaller radii. However, the saline specimen has a

287 significant fraction of larger pores with radii ranging from 1 to 10  $\mu\text{m}$ , which is not present in the  
 288 distilled water specimen. This is consistent with the interpretation provided for the fabric of  
 289 Spigno Monferrati clay, that is characterized by larger voids in the presence of saline pore fluid.  
 290



291

292 Fig. 5 PSD curves of reconstituted Spigno Monferrato specimens prepared at their liquid limit  
 293 and loaded to 98 kPa.  
 294

295

### 296 3.3 Chemo mechanical loading paths: evidences on reconstituted Spigno 297 Monferrato clay

298

299 To investigate the combined effects of mechanical and chemical solicitations, a chemo-  
 300 mechanical loading path was imposed on a reconstituted specimen of Spigno Monferrato clay,  
 301 according to the sequence shown in Figure 6, while the experimental results in the compression  
 302 plane are provided in Figure 7. A slurry specimen was prepared using distilled water to obtain an  
 303 initial void ratio  $e_0 = 1.2 e_L$  and then placed in an oedometer.

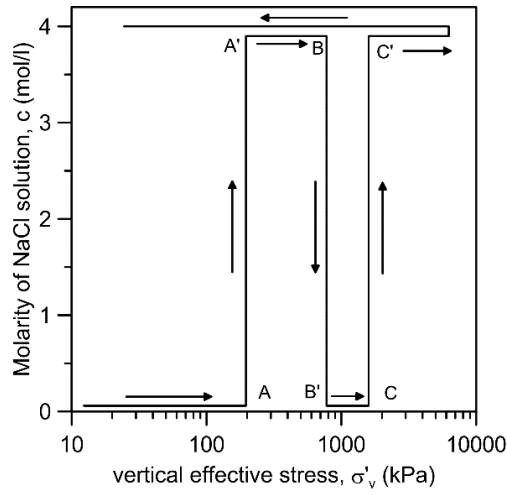
304 Distilled water was poured in the oedometer cell and mechanical loading was applied by doubling  
305 the vertical stress every 24 hours up to  $\sigma'_v = 196$  kPa (point A in Figures 6 and 7). This vertical  
306 stress was kept for 24 hours and then the fluid in the cell was replaced with a 4 M NaCl solution,  
307 renewed daily to ensure constant salt concentration of the pore fluid at the boundary of the  
308 specimen. The slow process of cation diffusion from the oedometer cell to the interior of the  
309 specimen caused volume change to occur along time (i.e. osmotic consolidation, according to  
310 Barbour & Fredlund, 1989). The corresponding volumetric strain took place in about 1 week. As  
311 it can be appreciated in Figure 7, a decrease in void ratio occurred (Point A' in Figures 6 and 7).  
312 To remove the effects that imparted by creep (as suggested by Torrance, 1974), in Figure 7 the  
313 void ratios under the mechanical loads refer to the end of mechanical consolidation, while the  
314 changes in void ratio measured during the chemical loads were corrected removing the effects  
315 of secondary compression, expected to grow linearly with the logarithm of time.

316 A mechanical loading sequence started again with the saline solution as pore and cell fluid. Small  
317 stress increments were initially applied to appreciate possible effects of the chemical history on  
318 the mechanical behaviour, i.e. to detect as precisely as possible any change in preconsolidation  
319 pressure. Under a vertical effective stress  $\sigma'_v = 780$  kPa (point B), the procedure was inverted and  
320 the cell fluid was replaced with distilled water, renewed daily to ensure constant fluid  
321 composition at the specimen boundary. As long as the NaCl ions diffused outside of the specimen,  
322 the specimen progressively shrank and the void ratio reduced (point B' in Figures 6 and 7). Load  
323 increments were then imposed at constant pore fluid composition, again paying attention to the  
324 identification of preconsolidation pressure evolution. Another salinisation step was performed  
325 under a vertical effective stress  $\sigma'_v = 1600$  kPa with a small decrease in the void ratio from

326  $e = 0.59$  to  $e = 0.58$  (points C and C'). The following loading and unloading were performed at  
327 constant salinity.

328 As evident from Figure 7, the stress increments which immediately followed the first salinisation  
329 were characterised by an increase in stiffness (i.e. smaller compliance) with respect to the  
330 previous ones, so the experimental points do not align with the projection of the compression  
331 line deduced for the previous steps with distilled water as saturating fluid. A larger compliance  
332 was recorded again for the stress increment between 600 and 780 kPa. Salinisation appears thus  
333 to provide a sort of preconsolidation, causing an apparent OCR of the order of 2.5 – 3. A small  
334 preconsolidation effect also occurred with the salinization step imposed at  $\sigma'_v = 1600$  kPa. On  
335 the other hand, after desalinisation (e.g. between points B' and C) the compliance that was  
336 registered immediately is comparable to one of the virgin material, and no preconsolidation  
337 effects were observed.

338 It is interesting to observe that, on the compression plane, the points which correspond to  
339 saturation with distilled water align reasonably well along a certain Normal Compression Line.  
340 The 'normally consolidated' points (i.e. for which the apparent OCR is 1) of the 4 M NaCl condition  
341 align instead along another NCL. The position of the NCL of the specimen that was prepared and  
342 loaded with the 4 M NaCl solution is also drawn in Figure 7. It can be appreciated that the NCL  
343 for the condition of preparation with distilled water and loading with 4 M NaCl lays between the  
344 NCL of preparation and loading with distilled water and the NCL of preparation and loading with  
345 brine.  
346



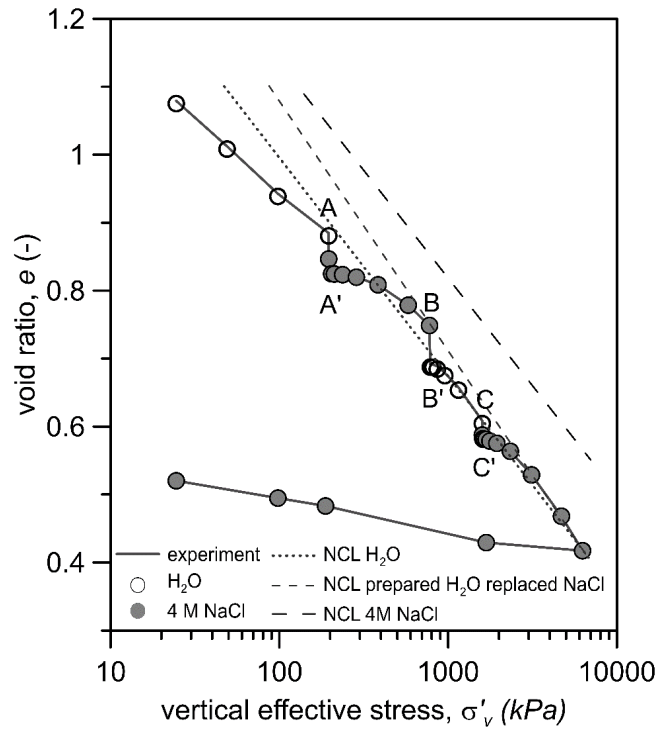
347

348

Fig. 6 Chemo-mechanical loading path imposed to reconstituted Spigno Monferrato clay

349

350



351

Fig. 7 Compression curves of reconstituted Spigno Monferrato clay, subjected to chemo-mechanical loading path

352

353

354

## 355 **4 An elasto-plastic model for the chemo-** 356 **mechanical behaviour of non-expansive clays**

357

358 The experimental evidences collected in the previous sections provide the basis for the  
359 formulation of a simple phenomenological constitutive model capable of predicting the  
360 mechanical response of non - expansive clays subject to salinity changes. The model is developed  
361 in the framework of elasto-plasticity with generalized hardening (see, e.g.,  
362 Della Vecchia et al, 2013, Tamagnini & Ciantia, 2016). The role of pore fluid chemistry on the  
363 mechanical response is assumed to directly influence both the constitutive stress and the  
364 evolution of the internal state variable.

365

### 366 4.1 Stress variables

367

368 The model is based on the definition of a mechanical constitutive stress variable, to reproduce  
369 mechanical solicitations, and one environmental process variable to account for changes in the  
370 chemistry of the pore fluid. The mechanical variable is the Terzaghi effective stress tensor, with  
371 components  $\sigma'_{ij}$ :

372

$$373 \sigma'_{ij} = \sigma_{ij} - u\delta_{ij} \quad (3)$$

374

375 where  $\sigma_{ij}$  is the total stress,  $u$  is the pore fluid pressure and  $\delta_{ij}$  is the Kronecker's delta. The role  
376 of cation exchange is here neglected and the osmotic suction  $\pi$  is adopted as chemical process  
377 variable. The general expression for  $\pi$  is :

378

$$379 \quad \pi = -\frac{RT}{v_w} \ln(a_w) \quad (4)$$

380

381 where  $R$  is the universal gas constant ( $8.31 \text{ J mol}^{-1} \text{ K}^{-1}$ ),  $T$  is the absolute temperature,  $v_w$  is molar  
 382 volume of water and  $a_w$  is the activity of water, which depends on the concentration of dissolved  
 383 salts. At low concentrations the van't Hoff equation can be used:

384

$$385 \quad \pi = icRT \quad (5)$$

386

387 where  $i$  is the number of species in which the salt dissolves (e.g. 2 for NaCl and 3 for CaCl<sub>2</sub>) and  $c$   
 388 is the molar concentration of the electrolyte. For molar concentrations below 1 mole/liter, the  
 389 error introduced by van't Hoff equation is smaller than 5 % (Mitchell & Soga, 2005).

390 For the sake of simplicity, the usual volumetric and deviatoric decomposition of the stress and  
 391 strain tensor in axis-symmetric conditions is introduced in the following.

392

## 393 4.2 Elastic behaviour

394

395 Elastic volumetric strain increments are split into two contributions, one due to mechanical  
 396 loading,  $\varepsilon_{v\text{mec}}^e$  and the other due to osmotic suction changes,  $\varepsilon_{v\text{ch}}^e$ . The mechanical contribution  
 397 is defined evaluated through the logarithmic compliance  $\kappa$  adopted in critical state soil  
 398 mechanics. A similar parameter, the chemical elastic logarithmic compliance  $\kappa_\pi$ , is introduced to  
 399 evaluate the chemical component. The whole elastic volumetric strain increment  $\varepsilon_v^e$  then reads:

400

401 
$$\dot{\varepsilon}_v^e = \dot{\varepsilon}_{v\text{mec}}^e + \dot{\varepsilon}_{v\text{ch}}^e = \frac{\kappa \dot{p}'}{v p'} + \frac{\kappa \pi}{v} \frac{\dot{\pi}}{\pi + \pi_0}$$
 (6)

402

403 where  $v$  is the specific volume,  $\pi_0$  is a reference osmotic suction (e.g. 1 kPa) introduced to avoid  
 404 infinite values of  $v$  when  $\pi$  goes to zero and  $p'$  is the mean effective stress. The contribution of  
 405 osmotic suction to elastic shear strain is neglected, so that increment of elastic deviatoric strain  
 406  $\dot{\varepsilon}_s^e$  reads:

407 
$$\dot{\varepsilon}_s^e = \frac{1}{3G} \dot{q}$$
 (7)

408 where  $G$  is the (constant) shear modulus and  $q$  the deviator stress.

409

#### 410 4.3 Elastic-plastic behavior

411

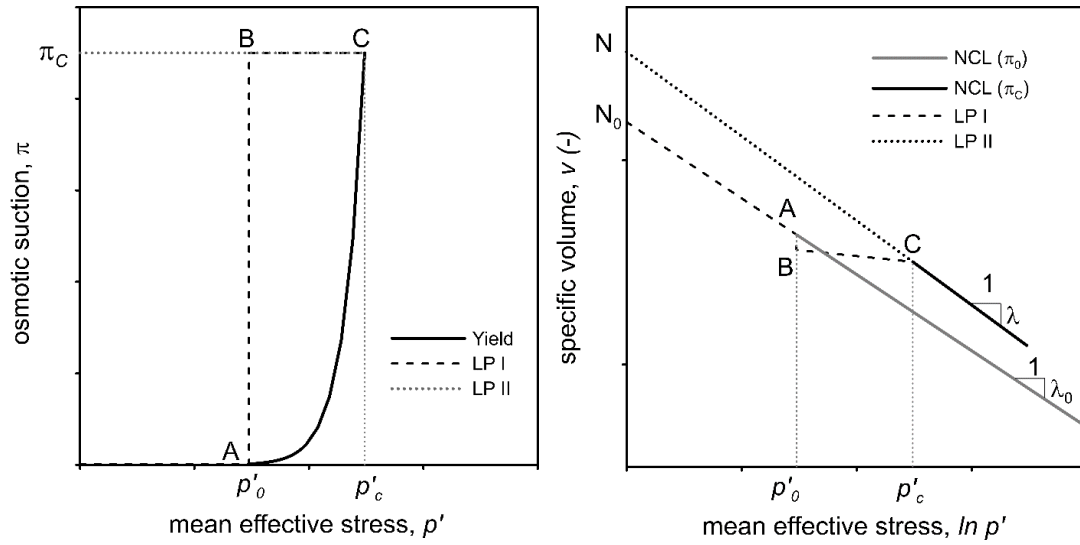
412 The yield surface in the  $(p', q, \pi)$  space is defined on basis of a simple mathematical interpretation  
 413 of the chemo-mechanical response in the compression plane. The approach followed is inspired  
 414 by the proposal of Alonso et al. (1990) to account for the role of matric suction on the behaviour  
 415 of unsaturated non-expansive soils.

416 As shown in the previous sections, the position and the slope of the NCL depend on the fabric  
 417 imparted by the history of mechanical and chemical loads. Both the parameters that identify the  
 418 NCL in the compression plane (the specific volume  $N$  for a reference mean effective stress  $p'_r$  and  
 419 the elasto-plastic logarithmic compliance  $\lambda$ ) may change with  $\pi$ . In the following,  $N_0$  and  $\lambda_0$  refer  
 420 to the soil saturated with distilled water, whereas  $N(\pi)$  and  $\lambda(\pi)$  refer to a generic saline solution  
 421 of osmotic suction  $\pi$ .

422 The preconsolidation pressure is expressed as  $p'_o$  when the soil is saturated with distilled water  
423 and it is expressed as  $p'_c(\pi)$  when the soil is saturated by the generic saline solution. The  
424 mathematical link between  $p'_o$  and  $p'_c$  can be obtained considering two different loading paths,  
425 LPI and LPII in the stress plane  $(p', \pi)$  of Figure 8a and in the compression plane  $(v, \ln p')$  of  
426 Figure 8b.

427 Along loading path LPI a sample 'prepared' and saturated distilled water is loaded in virgin  
428 conditions up to  $p'_o$  (point A): during this stage it moves along the NCL corresponding to  $\pi = 0$ .  
429 Osmotic suction is then increased to  $\pi = \pi_c$  while the mean effective stress is kept constant: this  
430 causes compressive elastic volumetric strains and the specific volume reduces (path AB in  
431 Figure 8). From B, the mechanical stress is further increased while the osmotic suction is kept  
432 constant. Elasto-plastic volume strains take place only when the specific volume lays on the NCL,  
433 thus volume contraction will initially be elastic as the NCL  $(\pi_c)$  lays above the NCL  $(\pi = 0)$ . Yielding  
434 occurs when the elastic reloading line meets the NCL  $(\pi_c)$ , i.e. at point C in Figure 8, where the  
435 mean effective stress is  $p'_c$  and the specific volume is  $v_c$ . By further increasing the mechanical  
436 stress, the behaviour will be elastoplastic and the sample will move along the NCL corresponding  
437 to  $\pi = \pi_c$ .

438 Point C can also be reached through the loading path LPII, corresponding to mechanical loading  
439 at constant osmotic suction  $\pi = \pi_c$  of a specimen that has the same fabric of C. In the compression  
440 plane, LPII marks the NCL  $(\pi_c)$  between  $p' = p'_r$  and  $p' = p'_c$ .



441 Fig. 8 a) Loading paths LPI and LPII and yield surface in the  $(p', \pi)$  plane; b) loading paths LPI and  
 442 LPII and Normal Compression Lines for the two different osmotic suctions  
 443

444 By evaluating  $v_c$  along LPI:

$$445 \quad v_c = N_0 - \lambda_0 \ln \left( \frac{p'_0}{p'_r} \right) + \Delta v^{ch} - \kappa \ln \left( \frac{p'_c}{p'_0} \right) \quad (8)$$

446 where  $\Delta v^{ch}$  is the elastic change in specific volume when the osmotic suction increases from 0  
 447 to  $\pi$ , evaluated with eq. (5):

$$448 \quad \Delta v^{ch} = -\kappa \pi \ln \left( \frac{\pi + \pi_0}{\pi_0} \right) \quad (9)$$

449 By evaluating  $v_c$  along LPII:

$$450 \quad v_c = N - \lambda \ln \left( \frac{p'_c}{p'_r} \right) \quad (10)$$

451 By introducing (8) in (7) and equating with (9), it follows:

$$452 \quad \frac{p'_c}{p'_0} = \left( \frac{p'_0}{p'_r} \right)^{\frac{\lambda_0 - \lambda}{\lambda - \kappa}} \cdot e^{\frac{N - N_0}{\lambda - \kappa}} \cdot \left( \frac{\pi + \pi_0}{\pi_0} \right)^{\frac{\kappa \pi}{(\lambda - \kappa)}} \quad (11)$$

453 Equation (10) provides the evolution of the yield mean stress  $p'_c$  with osmotic suction in isotropic  
 454 conditions. Extension to more general axis-symmetric conditions is performed through the yield  
 455 surface ( $f=0$ ) of the Modified Cam Clay model:

$$456 \quad f(p', q, p'_c) = \frac{q^2}{M^2} + p'(p' - p'_c) \quad (12)$$

457 where  $M$  is the slope of the Critical State Line in the  $(p', q)$ . The isotropic hardening law of the  
 458 Modified Cam Clay is used, with  $p'_0$  as the internal variable:

$$459 \quad \varepsilon_v^{pl} = \frac{\lambda_0 - \kappa}{v_0} \frac{p'_0}{p'_0} \quad (13)$$

460 where  $v_0$  is the specific volume associated to  $p'_0$ . An associated flow rule is finally adopted.

461 Suitable expressions relating  $N$  and  $\lambda$  to osmotic suction are also introduced. In analogy with what  
 462 observed for the liquid limits, whose evolution with concentration follows a logarithmic trend  
 463 (Figure 1), the following expressions are proposed:

$$464 \quad N(\pi) = N_0 + \beta \ln \left( \frac{\pi + \pi_0}{\pi_0} \right) \quad (14)$$

465

$$466 \quad \lambda(\pi) = \lambda_0 + \eta \ln \left( \frac{\pi + \pi_0}{\pi_0} \right) \quad (15)$$

467 where  $\beta$  and  $\eta$  are model parameters.

#### 468 4.4 Shape of the yield surface in the $(p', \pi)$ space

469

470 The shape of the yield function of eq. (11) in the  $(p', \pi)$  is controlled by:

471 (i) the dependency of  $\lambda$  on osmotic suction  $\left( \frac{p'_0}{p'_r} \right)^{\frac{\lambda_0 - \lambda}{\lambda - \kappa}}$ ,

472 (ii) the dependency  $N$  on osmotic suction  $e^{\frac{N - N_0}{\lambda - \kappa}}$ ;

473 (iii) the value of osmotic suction itself  $\cdot \left( \frac{\pi + \pi_0}{\pi_0} \right)^{\frac{\kappa \pi}{\lambda - \kappa}}$

474 These three factors depend on the mineralogy and initial fabric of the clay, so they might have  
 475 different relevance for different clays or clay “preparations”. For modelling purposes, two  
 476 simplified hypotheses might be of interest:

477 a) osmotic suction does not affect the position and the slope of the NCL. In this case eq. (10)  
 478 reduces to:

$$479 \quad \frac{p'_c}{p'_0} = \left( \frac{\pi + \pi_0}{\pi_0} \right)^{\frac{\kappa \pi}{\lambda_0 - \kappa}} \quad (16)$$

480 which points out the effects of the elastic chemical strains on the preconsolidation pressure;

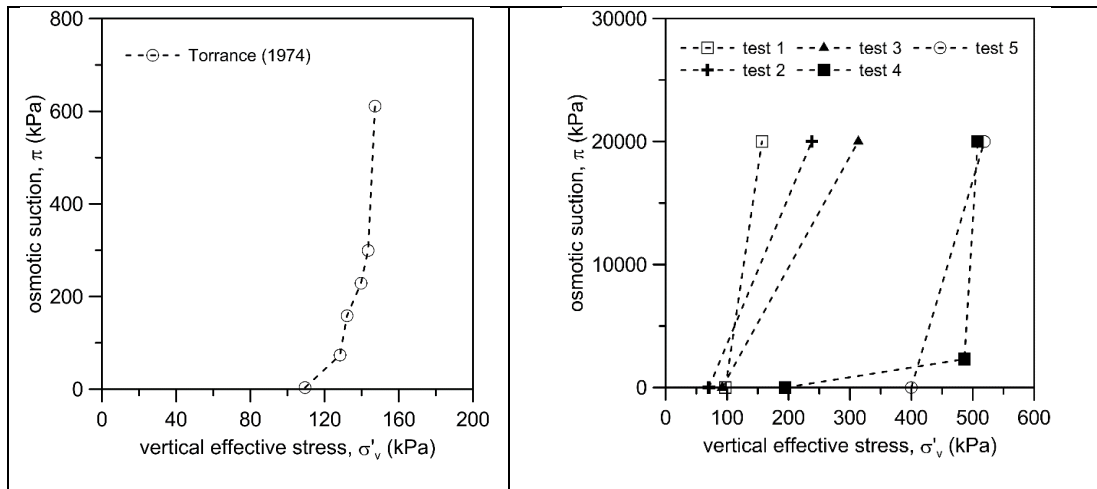
481 b) osmotic suction affects the position of the NCL but not its slope. According to Section 3,  
 482 this seems to be the case for many non-expansive clays. Eq. (10) reduces then to:

$$483 \quad \frac{p'_c}{p'_0} = e^{\frac{N - N_0}{\lambda_0 - \kappa}} \cdot \left( \frac{\pi + \pi_0}{\pi_0} \right)^{\frac{\kappa \pi}{\lambda_0 - \kappa}}, \quad (17)$$

484

485 The shape of the yield surface is consistent with the experimental evidences provided by  
 486 Torrance (1974) for Drammen clay and the ones collected in this study for Spigno Monferrato  
 487 clay, shown in Figure 9. Both cases refer to reconstituted samples prepared mixing the dry soil  
 488 powder with distilled water at a content higher than the liquid limit, and then loaded in the  
 489 oedometer according to the sequence LPI from Figure 8a.

490



491 Fig- 9. Experimental data of dependency of the preconsolidation pressure on osmotic suction: a)  
 492 Drammen clay (Torrance, 1974); b) Spigno Monferrato clay  
 493

## 494 5 Model validation for reconstituted, 495 compacted and undisturbed soils

496 Since the mechanical behaviour of a given soil depends on the fabric imparted at its formation,  
 497 the capabilities of the model were checked simulating oedometer tests performed on samples of  
 498 reconstituted, compacted and undisturbed clays. To this extent, the model was implemented in  
 499 a driver for the integration of the constitutive equations in rate form (see e.g.  
 500 Cattaneo et al., 2011, 2014). The driver allows imposing histories of prescribed chemo-  
 501 mechanical loading, which were assigned according with those adopted during the simulated  
 502 experiments. In all the simulations, the reference osmotic suction was imposed as  $\pi_0 = 1$  kPa.

503  
 504

## 505 5.1 Reconstituted Spigno Monferrato clay

506

507 The simulations of two oedometer tests run on reconstituted Spigno Monferrato clay were

508 performed. The values of the parameter used in the simulation are reported in Table 2.

509 Table 2 Parameters and initial value of  $p'_0$  used for the simulation of Spigno Monferrato clay

$\kappa$	$\lambda_0 = \lambda$	$\kappa_\pi$	$\nu$	M	$\beta$	$p'_0$
(-)	(-)	(-)	(-)	(-)	(-)	(kPa)
0.04	0.127	0.006	0.3	0.98	0.003	18

510

511  $\kappa$  and  $\lambda$  were calibrated on the compression response of a sample prepared and mechanically512 loaded with distilled water as cell fluid, while  $\kappa_\pi$  was calibrated on the volumetric strains due to

513 salinization of the first test described below. The dependence of N on pore fluid salinity was

514 simulated with  $\beta = 0.003$ . The slope of the critical state line  $M^*$  was set equal to 0.98 and as a

515 first approximation it was set independent from the chemical concentration of the pore fluid.

516 The two tests are characterized by different chemo-mechanical loading paths. The first one was

517 provided in Figure 6 (experimental results in Figure 7). The predictions of the model, shown in

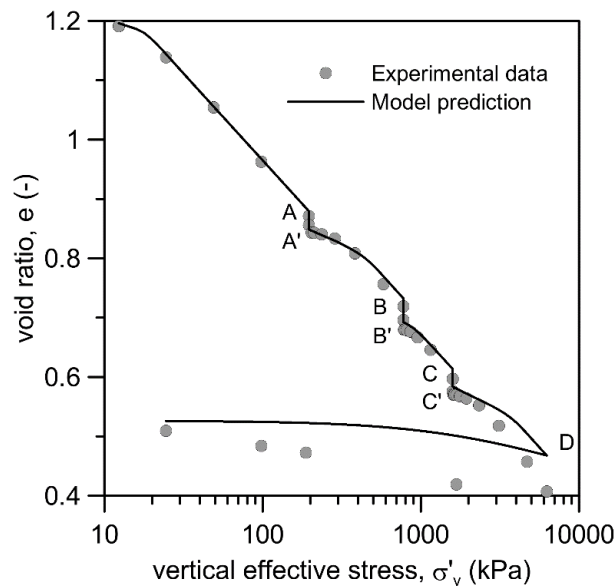
518 Figure 10, are in good agreement with the experimental data. The model is capable of predicting

519 volumetric shrinkage not only upon salinization (AA' and CC'), but also an irreversible void ratio

520 reduction upon desalinization (BB'). In accordance with experimental data, the convex shape of

521 the yield domain in the  $(p'-\pi)$  plane implies an elastic response due to mechanical loading after

522 salinization and an elasto-plastic response due to mechanical loading after desalinization.



523

524 Fig 10 – Results of the simulation of the chemo-mechanical loading path performed on Spigno  
 525 Monferrato clay of Figure 6.

526

527 The loading path in the salinity – vertical effective stress plane of the second oedometer test is

528 provided in Figure 11a. The material was prepared with distilled water and then loaded up to a

529 vertical stress  $\sigma'_v = 98$  kPa (point A in Figure 11), then unloaded to  $\sigma'_v = 74$  kPa (point B,

530 OCR = 1.3). Following the same procedure described in Sec. 3.3, the concentration of the

531 electrolyte in the cell fluid was increased to 4 M (NaCl) causing a decrease of volume up to point

532 B'. Finally, the specimen was loaded up to a vertical stress  $\sigma'_v = 6276$  kPa and finally unloaded to

533 24.5 kPa. The same parameters calibrated for the previous test were used in the simulation of

534 this test, apart from the initial preconsolidation pressure here set equal to  $p'_0 = 28$  kPa. The

535 model correctly predicts volumetric shrinkage upon salinization and the consequent increase in

536 preconsolidation pressure (Figure 11b), in very good agreement with the experimental data.

537

538

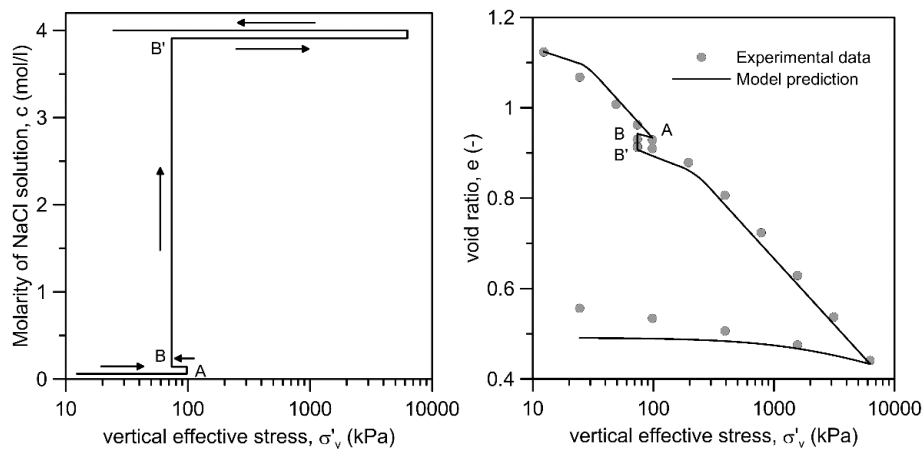


Fig 11 – (a) Loading path and (b) model predictions of the second chemo-mechanical test performed on Spigno Monferrato clay

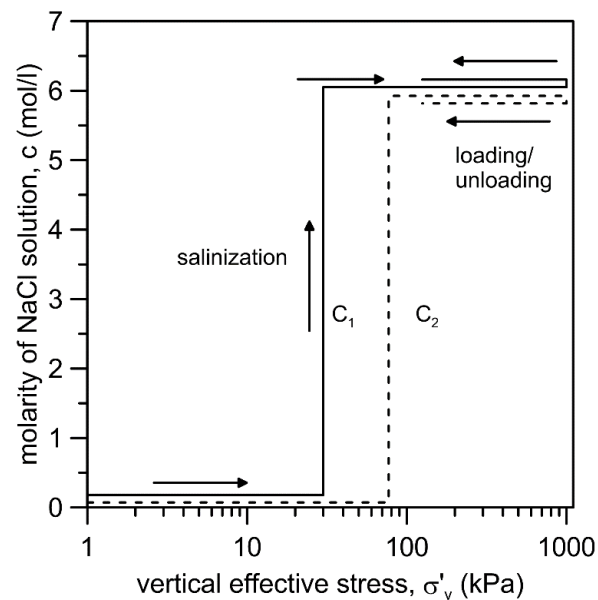
539  
540  
541  
542  
543  
544  
545

## 5.2 Compacted illitic clay (Witteveen et al., 2013)

546

547 The capability of the model to reproduce the behaviour of compacted clays was checked  
548 simulating two oedometer tests performed by Witteveen et al. (2013) on a compacted illitic soil  
549 (liquid limit  $w_L = 54\%$  and plasticity index  $PI = 24\%$ ). Specimens have been prepared by mixing  
550 the powder of the soil with distilled water at a water content below the liquid limit ( $w = 39\%$ )  
551 and statically compacted in oedometer up to different vertical stresses ( $\sigma'_v = 30$  kPa for test C1  
552 and  $\sigma'_v = 77$  kPa for test C2). According to the authors, water saturation was reached during static  
553 compaction. Under these vertical stresses the specimens have been exposed to a saturated NaCl  
554 saline solution: after suction equalization they have been loaded at constant suction to  
555  $\sigma'_v = 1000$  kPa and finally unloaded. The stress paths in the ( $\sigma'_v - M$ ) plane is shown in Figure 12.  
556 The parameters of the model were calibrated on the results of test C2 and then used to predicted  
557 the response for test C1: their values are provided in Table 3 together with the initial value of  $p'_0$ .  
558 The dependence of elasto-plastic compliance  $\lambda$  on pore fluid concentration was neglected, while  
559

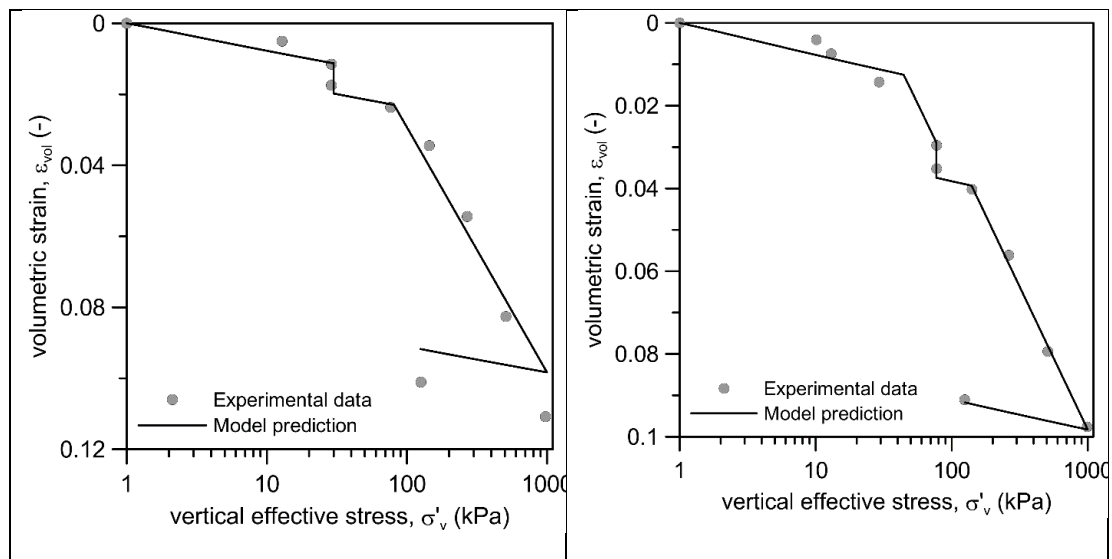
560 a small increase of  $N$  with osmotic suction was imposed ( $\beta = 0.0013$ ). The comparisons between  
 561 model predictions and experimental data are shown in Figure 13. The model proves able to  
 562 reproduce with a very limited number of parameters the main features of the chemo-mechanical  
 563 response on non-active clays, also if prepared by compaction. Remarkably, the obtained shape  
 564 of the yield function in the  $(p'-\pi)$  plane allows a correct prediction of the elastic reloading stage  
 565 if the material is loaded after salinization.  
 566



567

568 Fig 12. Chemo-mechanical loading path for compacted illitic soil (Witteveen et al, 2013)

569



570 Fig- 13. Comparison between experimental data and model predictions for compacted illitic soil  
 571 in Witteveen et al, 2013. Specimens C1 (left) and C2 (right).  
 572

573 Table 3 Parameters and initial value of  $p'_0$  used for the simulation of compacted illitic soil in  
 574 Witteveen et al. (2013)

$\kappa$ (-)	$\lambda_0$ (-)	$\kappa_\pi$ (-)	$G$ (kPa)	$M$ (-)	$\beta$ (-)	$p'_0$ (kPa)
0.006	0.058	0.0016	67	0.98	1.3 e-3	43

575

### 576 5.3 Intact and reconstituted quick clays

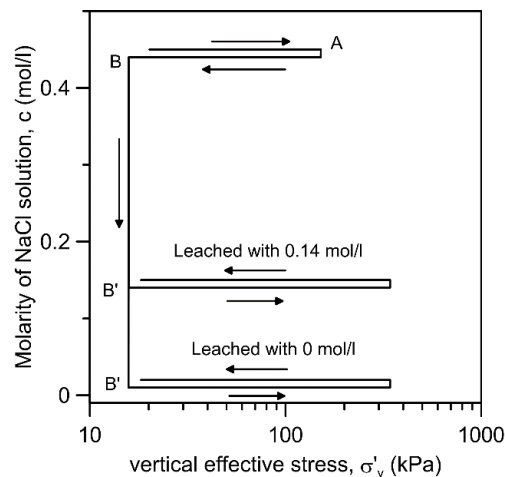
577

578 Torrance (1974) performed oedometer tests on undisturbed samples of intact Drammen clay, a  
 579 natural a low activity ( $w_L = 54\%$ ,  $IP = 23\%$ , Activity = 0.46) Norwegian quick clay, whose pore  
 580 water has an initial (natural) salt concentration of 26 g/l (Torrance 1974). Undisturbed specimens  
 581 have been loaded up to 150 kPa, a value larger than the in situ preconsolidation pressure, and  
 582 then unloaded to 15 kPa, inducing an OCR equal to 10. Afterwards, the specimens have been  
 583 subjected to leaching (i.e. the exposure to a fluid with a smaller saline concentration than the  
 584 initial one) at constant vertical stress. The fluids used for the leaching process have different NaCl

585 concentrations, namely 0, 1, 2, 3, 4 and 8 g/l. After leaching, specimens have been loaded again.  
 586 The loading path is shown in Figure 14 for leaching with 0 g/l and 8 g/l of NaCl ( $c = 0$  mol/l and  
 587  $c = 0.14$  mol/l respectively). Experimental results show desalinization-induced swelling and, upon  
 588 reloading, a reduction in the preconsolidation pressure with respect to the one induced by  
 589 previous loading. The entity of the reduction is larger the lower the salinity of the leaching fluid.  
 590 The results of the simulations referred to the specimens leached with 0 g/l and 8 g/l are reported  
 591 in Figure 15. The complete set of parameter values and the initial value of the  $p'_o$  used in the  
 592 simulation are reported in Table 4. Again, the dependence of  $\lambda$  on pore fluid concentration was  
 593 neglected, without compromising the quality of the numerical predictions. The model correctly  
 594 reproduces not only the elastic and elasto-plastic response upon mechanical loading, but also the  
 595 magnitude of swelling upon leaching.

596

597



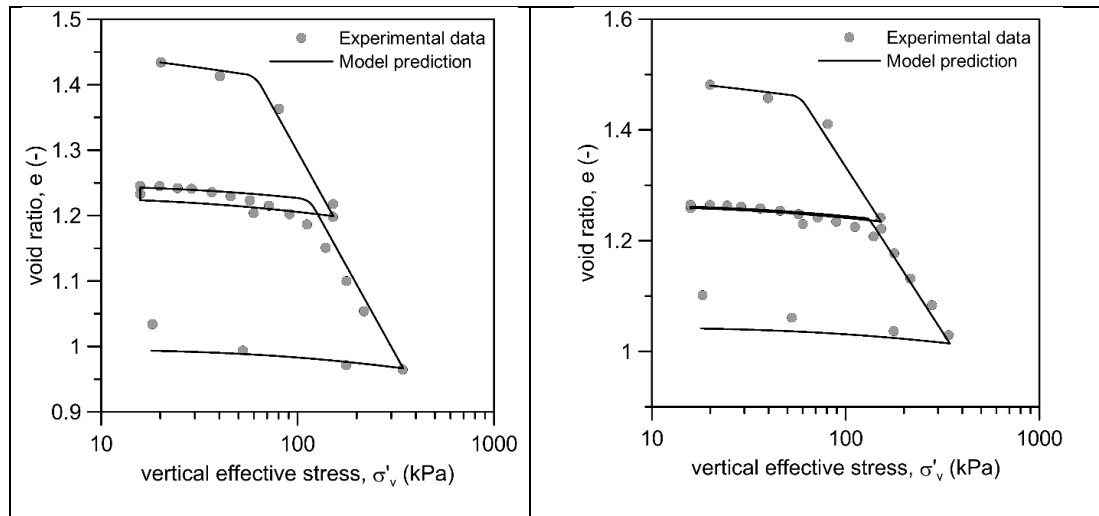
598

599

600

601

Fig- 14. Comparison between experimental data and model predictions for natural Drammen clay (experimental data from Torrance, 1974)



602 Fig- 15. Comparison between experimental data and model predictions for natural Drammen clay  
 603 (experimental data from Torrance, 1974). Leaching with distilled water (left) and with NaCl  
 604 solution with salt concentration 8 g/l (right)  
 605

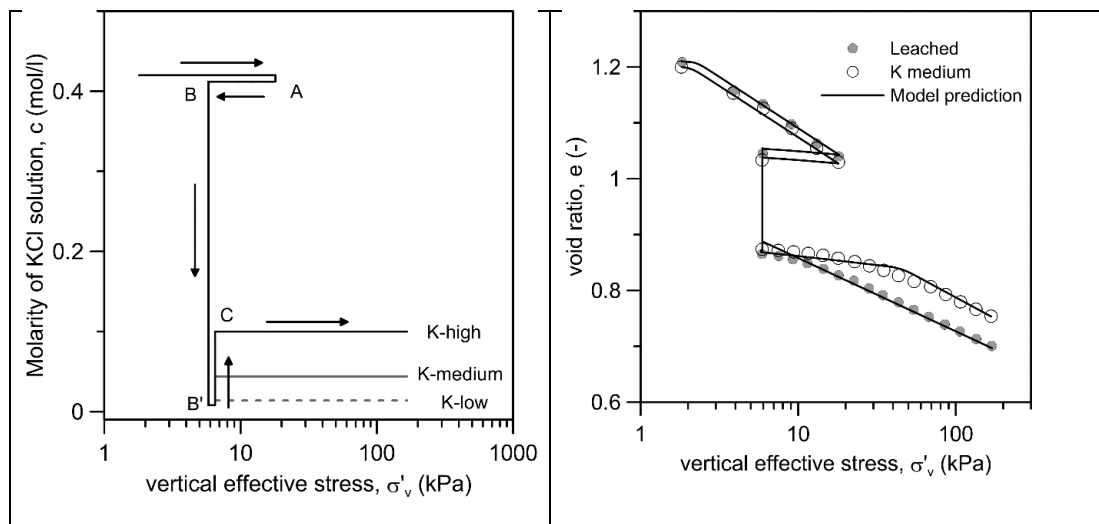
606 Table 4 Parameters and initial value of  $p'_0$  used for the simulation of natural Drammen clay

$\kappa$	$\lambda_0$	$\kappa_\pi$	$\nu$	M	$\beta$	$p'_0$
(-)	(-)	(-)	(-)	(-)	(-)	(kPa)
0.022	0.235	0.0031	0.3	0.98	4.8 e-3	39

607

608 A further validation of the model was performed against the results of oedometer tests on  
 609 Vaterland clay ( $w_L=40\%$ ,  $IP=16\%$ ,  $Activity=0.40$ ), another Norwegian quick clay (Torrance, 1974).  
 610 Four specimens of Vaterland marine clay had been remoulded with a NaCl solution of  
 611 concentration 26 g/L ( $c=0.44$  mol/l) as saturating fluid, loaded in oedometer to a vertical  
 612 effective stress  $\sigma'_v=18$  kPa (point A in Fig. 16 a), and then unloaded to  $\sigma'_v=6$  kPa (point B in  
 613 Fig. 16 a), inducing an OCR = 3. The specimens were then leached, i.e. exposed to distilled water  
 614 keeping the vertical stress constant (point B'): as consequence, the specimens experienced a  
 615 volume reduction. After leaching, three specimens had been exposed to potassium chloride at  
 616 different concentrations (namely K-low, K-medium and K-high, corresponding to 0.014 mol/l,

617 0.045 mol/l and 0.097 mol/l). One specimen, referred to as “leached specimen”, had only been  
 618 subjected to distilled water, without further changes in the pore fluid.  
 619 Afterwards, all the specimens had been reloaded to a vertical stress of 168 kPa. The loading paths  
 620 are shown in Figure 16 a, while the experimental data, as well as the model predictions, referring  
 621 to the leached specimen and to the specimen exposed to a medium concentration of potassium,  
 622 are shown in Figure 16 b.  
 623

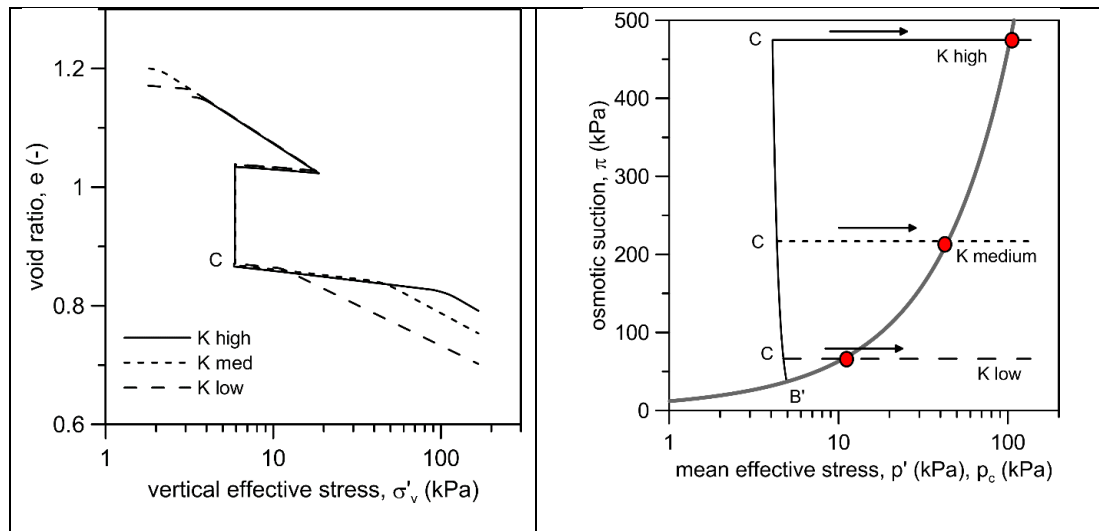


624 Fig- 16. Loading paths for Vaterland specimens leached with distilled water (BB') and then exposed  
 625 to potassium chloride (B'C) (left); comparison between experimental data and model predictions  
 626 for the leached specimen and for the specimen exposed to a medium concentration of potassium  
 627 chloride (right) (experimental data from Torrance, 1974)  
 628

629 The experimental data confirm that the normal compression lines interpolating the virgin  
 630 compression branches tend to shift upwards in the compression plane at increasing electrolyte  
 631 concentrations. The model proved able to reproduce the volumetric collapse caused by leaching  
 632 of moderately overconsolidated specimens and the simulations are in good agreement with the  
 633 experimental results. The dependence of  $\lambda$  on  $\pi$  (see eq. 15) was considered and the parameters

634 adopted in the simulations are reported in Table 5. The proposed framework consistently  
 635 predicts that the preconsolidation pressure depends on the history of both mechanical and  
 636 chemical loadings: indeed, after volumetric collapse the leached specimen behaved as a normally  
 637 consolidated material, while the K-medium specimen behaved as an overconsolidated material.  
 638 Figure 17a presents model predictions for the three specimens exposed to potassium chloride.  
 639 Due to the shape of the yield function which expands with osmotic suction (Figure 17b), the yield  
 640 stresses increase at increasing salt concentration.

641



642 Fig- 17. (a) Simulation of tests with potassium addition; (b) shape of yield function in  $p'$ - $\pi$  plane  
 643 during salinization (in bold black); stress paths referring to addition of potassium at different  
 644 concentrations and following reloading. Red points represent the intersection between the stress  
 645 path and the yield surface.

646  
647Table 5 Parameters and initial value of  $p'_0$  used for the simulation of Vaterland clay

$\kappa$ (-)	$\lambda_0$ (-)	$\kappa_\pi$ (-)	$\nu$ (-)	M	$\beta$ (-)	$\eta$ (-)	$p'_0$ (kPa)
0.015	0.04	0.003	0.3	0.98	0.045	0.002	1.0

648

## 649 **6 Conclusions**

650 The physico-chemical interaction between clay particles depends on the type of pore fluid and  
651 the mineralogy of the clay. The fabric of natural and reconstituted non-expansive illitic and  
652 smectitic clays in distilled water is mostly related to particle aggregation without flocculation,  
653 whereas it shows flocculation of particles or aggregates of particles in presence of dissolved salts.  
654 The flocculated fabric persists also when the stress is increased, whereas it is at least partially  
655 destroyed upon desalinization. The flocculated fabric is associated to larger pores with respect  
656 to the aggregated one, which helps explaining the experimental evidences that show the NCL of  
657 these soils moving to higher void ratios as the salt content increases. Changes in pore chemistry  
658 occurring under constant stress cause similar movements of the NCL, although to a limited  
659 extent. Even if the fabric of compacted soils is dominated by the effects of the mechanical load  
660 imparted in unsaturated conditions during compaction, the same effects seems to occur also for  
661 these soils. While changes in the thickness of the DDL alone would suggest an elastic type of  
662 behaviour, with volume contraction upon salinity increase and expansion upon salinity decrease,  
663 the experimental evidence shows that in normally consolidated non-expansive clays  
664 desalinitisation leads to inelastic compressive volume strains (collapse). These evidences at the  
665 phenomenological level resemble those observed for non-active unsaturated soils exposed to a  
666 decrease in matric suction. Their critical analysis lead to the proposal of an elasto-plastic model,  
667 which was formulated following the same procedure adopted by [Alonso et al. \(1990\)](#) for the  
668 Barcelona Basic Model (BBM). A yield function which expands with osmotic suction, governed by  
669 the elastic chemical compressibility and the variations in the position and slope of the NCL,  
670 follows naturally from this procedure. The role of such a yield function with respect to chemo-

671 mechanical plastic effects is analogous to the one played by the Loading Collapse (LC) in the BBM.  
 672 However, it is worth noting that the LC for unsaturated soils and the present yield function (eq.  
 673 10) account for different physical processes (LC for capillarity and the present one for salinity,  
 674 mediated through changes in fabric arrangements discussed previously).

675

## 676 Acknowledgments

677 The first author would like to acknowledge the contributions of Francesco Macario, MSc. and of  
 678 Mattia Minnite, Msc., which carried out the tests on Spigno Monferrato clay and on Illite. Thanks  
 679 are due also to Andrea Barillaro, geologist of BAAN Industrial Raw Materials, for providing the  
 680 pure Illite powder.

681

## 682 Notation

$a_w$	activity of water
$c$	molar concentration
$e_L$	void ratio at liquid limit with saline solution as saturating fluid
$e_L^0$	void ratio at liquid limit with distilled water as saturating fluid
$i$	number of species of the solute
$M$	slope of the Critical State Line in the $(p', q)$ plane
$N$	intercept of the Normal Compression Line
$N_0$	Intercept of the Normal Compression Line with distilled water

$p'$	mean effective stress
$p'_c$	preconsolidation pressure
$p'_r$	reference mean stress
$p'_o$	preconsolidation pressure with distilled water
$q$	deviatoric stress
$R$	universal gas constant
$T$	absolute temperature
$u$	pore pressure
$v$	specific volume
$v_w$	molar volume of H <sub>2</sub> O
$\beta$	model parameter describing the dependency of $N$ on osmotic suction
$\delta_{ij}$	Kronecker delta
$\dot{\epsilon}_s^e$	increment of deviatoric strain
$\dot{\epsilon}_{v\ ch}^e$	increment of elastic volume strain due to osmotic suction change
$\dot{\epsilon}_{v\ mec}^e$	increment of elastic volume strain due to stress change
$\dot{\epsilon}_v^e$	increment of elastic volume strain
$\eta$	model parameter describing the dependency of $\lambda$ on osmotic suction
$\kappa$	elastic logarithmic mechanical compliance
$\kappa_\pi$	chemical elastic compliance
$\lambda$	elasto-plastic logarithmic mechanical compliance
$\lambda_0$	elasto-plastic logarithmic compliance at reference osmotic suction
$\pi$	osmotic suction

$\pi_0$	reference osmotic suction
$\sigma_{ij}$	component of total stress
$\sigma'_{ij}$	component of Terzaghi effective stress

683

684

685 **References**

- 686 Alonso EE, Gens A, and Josa A (1990) A constitutive model for partially saturated soils.  
687 *Géotechnique* **40(3)**: 405–430.
- 688 Barbour SL and Fredlund DG (1989) Mechanisms of osmotic flow and volume change in clay soils.  
689 *Canadian Geotechnical Journal* **26(4)**: 551–562.
- 690 Barbour SL and Yang N (1993) A review of the influence of clay-brine interactions on the  
691 geotechnical properties of Ca-montmorillonitic clayey soils from western Canada. *Canadian*  
692 *Geotechnical Journal* **30(6)**: 920–934.
- 693 Bjerrum L and Rosenqvist IT (1956) Some experiments with artificially sedimented clays.  
694 *Géotechnique* **6 (4)**: 124–136.
- 695 Cattaneo F Della Vecchia G and Jommi C (2011) A driver for the integration of coupled hydro-  
696 mechanical constitutive laws for unsaturated soils. In *Unsaturated soils: Proceedings of the Fifth*  
697 *International Conference on Unsaturated Soils. Barcelona* (Alonso EE and Gens A (eds)). Balkema,  
698 Rotterdam, The Netherlands, vol. 2, pp 1017-23.
- 699 Cattaneo F, Della Vecchia G and Jommi, C (2014) Evaluation of numerical stress-point algorithms  
700 on elastic–plastic models for unsaturated soils with hardening dependent on the degree of  
701 saturation. *Computers and Geotechnics* **55**: 404-415.
- 702 Collins KT and McGown A (1974). The form and function of microfabric features in a variety of  
703 natural soils. *Géotechnique* **24(2)**: 223–254.
- 704 Di Maio C (1996). Exposure of bentonite to salt solution: osmotic and mechanical effects.  
705 *Géotechnique* **46(4)**: 695-707.

- 706 Di Maio C, Santoli L and Schiavone P (2004) Volume change behaviour of clays: the influence of  
707 mineral composition, pore fluid composition and stress state. *Mechanics of Materials* **36**: 435–  
708 451.
- 709 Della Vecchia G, Jommi C and Romero E (2013). A fully coupled elastic–plastic hydromechanical  
710 model for compacted soils accounting for clay activity. *International Journal for Numerical and*  
711 *Analytical Methods in Geomechanics*, **37(5)**: 503-535.
- 712 Della Vecchia G and Musso G (2016). Some remarks on single-and double-porosity modeling of  
713 coupled chemo-hydro-mechanical processes in clays. *Soils and Foundations* **56(5)**: 779-789.
- 714 Della Vecchia G Scelsi G and Musso G (2019) Modelling the role of pore water salinity on the  
715 water retention behaviour of compacted active clays. *Italian Geotechnical Journal (Rivista Italiana*  
716 *di Geotecnica)*, **3**: 16-19
- 717 Gajo A and Loret B (2003). Finite element simulations of chemo-mechanical coupling in elastic–  
718 plastic homoionic expansive clays. *Computer Methods in Applied Mechanics and Engineering*  
719 **192(31-32)**: 3489-3530.
- 720 Guimarães L D N, Gens A, Sánchez M and Olivella, S (2013). A chemo-mechanical constitutive  
721 model accounting for cation exchange in expansive clays. *Géotechnique* **63(3)**: 221-234.
- 722 Hueckel T (1997) Chemo-plasticity of clays subjected to stress and flow of a single contaminant.  
723 *International Journal for Numerical and Analytical Methods in Geomechanics* **21(1)**: 43–72.
- 724 Jang, J and Santamarina, J C (2016). Fines classification based on sensitivity to pore-fluid  
725 chemistry. *Journal of Geotechnical and Geoenvironmental Engineering ASCE* **142(4)**: 06015018

- 726 Liu Z, Boukpeti N, Li X, Collin F, Radu J P, Hueckel T, and Charlier R (2005). Modelling chemo-  
727 hydro-mechanical behaviour of unsaturated clays: a feasibility study. *International Journal for*  
728 *Numerical and Analytical Methods in Geomechanics*, **29(9)**: 919-940.
- 729 Loret B, Hueckel T and Gajo A (2002). Chemo-mechanical coupling in saturated porous media:  
730 elastic–plastic behaviour of homoionic expansive clays. *International Journal of Solids and*  
731 *Structures* **39(10)**: 2773-2806.
- 732 Mitchell, J K and Soga, K (2005). *Fundamentals of soil behavior*. Wiley.
- 733 Musso G, Romero E, Gens A, and Castellanos E (2003). The role of structure in the chemically  
734 induced deformations of Febex bentonite. *Applied Clay Science*, **23(1-4)**: 229–237.
- 735 Musso G, Chighini S and Romero E (2008). Mechanical sensitivity to hydrochemical processes of  
736 Monastero Bormida clay. *Water Resources Research*, **44(5)**: W00C10.
- 737 Musso G, Romero E, and Della Vecchia G (2013). Double-structure effects on the chemo-hydro-  
738 mechanical behaviour of a compacted active clay. *Géotechnique*, **63(3)**: 206-220.
- 739 Musso G, Cosentini RM, Dominijanni A, Guarena N and Manassero M (2017). Laboratory  
740 characterization of the chemo-hydro-mechanical behaviour of chemically sensitive clays. *Italian*  
741 *Geotechnical Journal (Rivista Italiana Di Geotecnica)*, **3**:22–47.
- 742 Noorany, I (1984) Phase relations in marine soils. *Journal of Geotechnical Engineering*  
743 **ASCE 110(4)**: 539 - 543
- 744 Ohtsubo M, Egashira K and Takayama M (1985). Properties of a low-swelling smectitic marine  
745 clay of interest in soil engineering. *Canadian Geotechnical Journal*, **22(2)**: 241-245.
- 746 Palomino AM and Santamarina J C (2005). Fabric map for kaolinite: effects of pH and ionic  
747 concentration on behaviour. *Clays and Clay Minerals*, **53(3)**: 211-223.

- 748 Rosenqvist, IT (1966). Norwegian research into the properties of quick clay—a review.  
749 Engineering Geology, **1(6)**: 445-450.
- 750 Santamarina JC, Klein KA and Fam MA (2001). *Soils and waves: Particulate materials behavior,*  
751 *characterization and process monitoring*. Wiley.
- 752 Santamarina JC, Klein KA, Palomino A and Guimaraes MS (2002). Micro-scale aspects of chemical-  
753 mechanical coupling: Interparticle forces and fabric. In *Chemo-Mechanical coupling in clays: From*  
754 *nano-structure to engineering applications, Maratea*. (Di Maio C, Hueckel T and Loret B (eds)).  
755 Balkema, Rotterdam, The Netherlands, pp. 47–64.
- 756 Sposito, G (1984). *The surface chemistry of soils*. Oxford University Press
- 757 Sridharan A and Rao GV (1973). Mechanisms controlling volume change of saturated clays and  
758 the role of the effective stress concept. *Géotechnique*, **23(3)**: 359–382.
- 759 Sridharan A, Rao S and Murthy N (1986) Liquid limit of montmorillonite soils. *Geotechnical*  
760 *Testing Journal*, **9(3)**: 156-159.
- 761 Sridharan A, Rao S and Murthy N (1988) Liquid limit of kaolinitic soils. *Géotechnique*, **38(2)**: 191-  
762 198
- 763 Sridharan, A (1991). Engineering behaviour of fine grained soils. A fundamental approach. *Indian*  
764 *Geotechnical Journal*, **21(2)**: 133-144.
- 765 Tamagnini C and Ciantia M (2016). Plasticity with generalized hardening: constitutive modeling  
766 and computational aspects. *Acta Geotechnica*, **11(3)**: 595–623.
- 767 Torrance, JK (1974). A laboratory investigation of the effect of leaching on the compressibility  
768 and shear strength of Norwegian marine clays. *Géotechnique* **24(2)**: 155-173.

- 769 Torrance JK and Ohtsubo M (1995) Ariake bay quick clays: a comparison with the general model.  
770 *Soils and Foundations*, **35(1)**: 11-19.
- 771 Van Olphen, H (1977) *An introduction to clay colloid chemistry, for clay technologists, geologists,*  
772 *and soil scientists*. 2nd edition, Wiley
- 773 Witteveen P, Ferrari A and Laloui L (2013) An experimental and constitutive investigation on the  
774 chemo-mechanical behavior of a clay. *Géotechnique*, **63(3)**: 244-255.
- 775 Yan, R (2018). BBM-type constitutive model for coupled chemomechanical behavior of saturated  
776 soils. *ASCE International Journal of Geomechanics*, **18(10)**: 06018023.